THE JOURNAL OF PHYSICAL CHEMISTRY C

ARTICLE

pubs.acs.org/JPCC

Rectification of the Current in α-Hemolysin Pore Depends on the Cation Type: The Alkali Series Probed by Molecular Dynamics Simulations and Experiments

Swati Bhattacharya,[†] L. Muzard,[‡] L. Payet,[§] Jerome Mathé,[§] Ulrich Bockelmann,[‡] Aleksei Aksimentiev,*[,∥] and Virgile Viasnoff*[,‡]

[†]Department of Physics and Beckman Institute, University of Illinois, Urbana, Illinois 61820, United States

[‡]Ecole Supérieure de Physique et Chimie Industrielles, ParisTech, Centre National de la Recherche Scientifique, France

[§]LAMBE-MPI, Univ. Evry val d'Essonne, Centre National de la Recherche Scientifique, Evry, France

[∥]Department of Physics, Beckman Institute, University of Illinois, Urbana, Illinois 61820, United States

Supporting Information

ABSTRACT: A striking feature of the α-hemolysin channel—a prime candidate for biotechnological applications—is the dependence of its ionic conductance on the magnitude and direction of the applied bias. Through a combination of lipid bilayer single-channel recording and molecular dynamics (MD) simulations, we characterized the current−voltage relationship of α-hemolysin for all alkali chloride salts at neutral pH. The rectification of the ionic current was found to depend on the type of cations and increase from Li^+ to Cs^+. Analysis of the MD trajectories yielded a simple quantitative model that related the ionic current to the electrostatic potential, the concentration and effective mobility of ions in the channel. MD simulations reveal that the major contribution to the current asymmetry and rectification properties originates from the cationic contribution to the current that is significantly reduced in a cationic-dependent way when the membrane polarity is reversed. The variation of chloride current was found to be less important. We report that the differential affinity of cations for the charged residues positioned at the channel's end modulates the number of ions inside the channel stem, thus affecting the current properties. Through direct comparison of simulation and experiment, this study evaluates the accuracy of the MD method for prediction of the asymmetric, voltage-dependent conductances of a membrane channel.

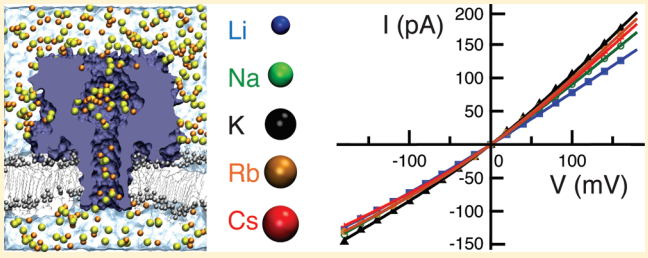

INTRODUCTION

Transport of ions through nanometer-size pores is a process ubiquitous in both biology and nanotechnology. In a biological cell, the concentration of ions is maintained by membrane proteins that either utilize chemical energy to actively transport ions across the biological membranes or passively transport ions along the gradient of the electrochemical potential.[1] Despite its conceptual simplicity, passive transport plays a major role in the biology of a living cell and can be selective, unidirectional, and voltage or ligand gated—the functionality furnished by specific ion−protein interactions.

Mimicking nature, synthetic nanoporous membranes have been designed to exhibit size and charge exclusion for specific molecules. Thus, nanopores in polymer[2] or solid-state[3] membranes have been fabricated to display diode-like behavior attributed to surface charge effects.[4,5] Proteinaceous[6−8] or synthetic[9−13] nanopores have been used as single molecule sensors that detect the presence of a macromolecule as a transient reduction of the ionic current flowing through the nanopore.[14] By comparing the residual ionic currents for the states associated with the presence of macromolecules in the nanopores, several types of macromolecules could be discriminated.[15,16] In general, the nanopore current depends on the shape of the nanopore,[17−19] the pH of the electrolyte,[20] the local distribution of surface charges,[21−24] denaturing condition[25] and the chemical nature of the ions, which is the focus of this study. Understanding the effect of ion type on the mechanism of transmembrane transport is of general interest not only because of its biophysical relevance but also for its potential utility in rational design of nanopore sensors.

A striking feature of many biological channels is their ability to rectify ($I(+V) \neq I(-V)$) the ionic current. This effect has been the subject of extensive experimental,[20] theoretical,[26−33] and computational[33−38] studies. More than 120 years ago, Nernst and Planck provided a theoretical framework for describing the effect of the electrostatic potential on ion transport. Furthermore, the Poisson equation allows the distribution of the electrostatic potential to be computed self-consistently with the local

Received: December 1, 2010
Revised: January 24, 2011

   dx.doi.org/10.1021/jp111441p | J. Phys. Chem. C XXXX, XXX, 000–000

Table 1. Parametrization of the Electric Circuit Model, Equation 1, Used to Fit the Experimental $I-V$ Curves[a]

cations	σ_b (mS/cm)	I_o (pA)	V_o (mV)	$G_{-\infty}$	$G_{+\infty}$	$(G_{+\infty})/(\sigma_b)$ (Å)
Li^+	74.2	28	1.6	0.67	0.80	1.1
Na^+	85.3	31	4.9	0.69	0.97	1.1
K^+	108	24	4.0	0.75	1.15	1.0
Rb^+	109	32	7.4	0.65	1.11	1.0
Cs^+	109	23	5.9	0.63	1.06	0.97

[a] $G_{-\infty} = (1)/(R + r)$ and $G_{\infty} = (1/R)$ are the values of the pore conductance at large negative and positive voltages, respectively. Notice that $G_{-\infty}$ hardly depends on the ion type, whereas G_{∞} scales with the bulk conductivity.

ion concentration. This so-called Poisson−Nernst−Planck approach, however, does not take into account the chemical nature of ions except for their mobility, as it considers ions as point charges. Moreover, the distribution of charges in a biological channel is often discrete and reflects the presence of charged residues at the channel's surface. Thus, the influence of a charged residue on the ionic current may strongly depend on the exact location of the residue in the pore. Accurate estimates of the interactions between single ions and individual residues of the channel are therefore critical for the development of quantitative models of ionic transport. The validity of the mean-field approximation in such cases has been called into question.[39] In the case of α-hemolysin, molecular dynamics (MD) simulations have proven sufficiently accurate to reproduce the asymmetric current−voltage dependence of KCl buffer.[35] Brownian dynamics simulations[33,34] and site-directed mutagenesis[40] have identified aspartate residues at the *trans* end of the channel as a major determinant of the rate of K^+ transport.

In this manuscript, we investigate the molecular origin of the dependence of the current rectification on the chemical nature of cations. By means of lipid bilayer single-channel recording, we characterize the voltage-dependent conductance of α-hemolysin for all cations from the alkali series: (Li^+, Na^+, K^+, Rb^+, Cs^+). First, we experimentally show that the conductance of α-hemolysin is modified in a nontrivial way when the type of cations is changed. In particular, we find the rectifying properties of the channel to depend on the cation type. Next, we show that MD simulations of the channel conductance are in quantitative agreement with our experimental data. Finally, quantitative analysis of the MD trajectories reveals the molecular origin of the cation-type-dependent rectification of the ionic current: the depletion of mobile cations in the channel's stem caused by interactions with charged residues of the pore.

MATERIAL AND METHODS

Experiment. Alkali chloride powders were purchased anhydrous from Sigma and dried under vacuum overnight before dilution. Salt buffers (1 M) were prepared in 100 mM tris at pH 7.4. The solution conductivities were measured at 24 °C. The measured conductivities were in agreement with the values found in the literature and are listed in Table 1.

To measure the $I-V$ curves of a single α-hemolysin pore under symmetric buffer conditions, we used a classical setup described previously.[41] DPPC lipids (Avanti Lipids) were used to form a suspended bilayer. The ionic current and the applied voltage were measured synchronously using AxoPatch 200B and a National Instrument acquisition board. Single pores spontaneously inserted into the lipid bilayer at a rate that did not noticeably depend on the buffer. The pore stability typically exceeded one hour with no gating or large fluctuations of the current at 120 mV. By convention, the pore vestibule (*cis* side) was grounded, and the stem side (*trans* side) held at a fixed potential. All experiments were performed under symmetric salt conditions. A symmetric triangle wave with an amplitude of 180 mV and a frequency of 1 Hz was applied to measure the $I-V$ curves . The measured current had two components: the current determined by the resistance of the pore and the capacitive current caused by charging of the lipid membrane with a rate of 0.72 V s^{-1}: $i_c = C(dV)/(dt)$. The latter component was removed by averaging $I-V$ curves measured during charging and discharging of the membrane. Adjustments smaller than 1 pA were necessary to ensure the ionic current is null at a zero bias voltage.

All $I-V$ curves measured using the same pore were perfectly reproducible, at least over a period of 30 min. A typical variation in the $I-V$ curves between measurements performed using 54 different pores was ±7.5%. We attribute such variability in the current to small variations in the structure of the self-assembled α-hemolysin heptamer, although the effect of buffer evaporation could not be fully excluded. Normalizing the $I-V$ curves with the current value obtained at any positive voltage bias reduced the variation to ±0.95%. All experimental $I-V$ curves reported in this study were obtained by averaging the data over 10−20 pores causing a statistical uncertainty in the current values of 2%.

Simulation. All MD simulations were performed using NAMD,[42] periodic boundary conditions, the particle mesh Ewald summation method for long-range electrostatics,[43] and multiple time stepping.[42,44] Local interactions were calculated every step, and full electrostatic evaluations were performed every 3 time steps. The van der Waals forces were evaluated using a cutoff of 8 Å and a switching distance of 7 Å.[45] Bonds and angles in water molecules were kept rigid using SETTLE,[46] while all other covalent bonds with hydrogen were kept rigid using RATTLE,[47] which allowed for a time step of 2 fs. The standard CHARMM27 parameters[48] were used to describe lipid, protein, and water along with the CHARMM-compatible parameter set for the entire series of alkali ions.[49]

The all-atom models of α-hemolysin suspended in a lipid bilayer membrane were built as described previously.[35] The atomic coordinates of the protein were obtained from the Protein Data Bank (entry 7AHL).[50] After adding missing atoms and residues, the structure was embedded in a patch of pre-equilibrated DPPC lipid bilayer. The protein−lipid complex was then solvated in a rectangular volume of ∼59 000 pre-equilibrated TIP3P water molecules.[51] The alkali (Li^+, Na^+, K^+, Rb^+, Cs^+) and chloride ions were added at random positions corresponding to a concentration of 1 M with additional charges to neutralize the system. The total system consisted of about 289 000 atoms and measured 13.2 × 13.4 × 15.6 nm^3. Three mutant pores were constructed, with Asp127, Asp128 or Asp127, Asp128, and Lys131 residues neutralized by applying corresponding protonation/deprotonation patches. Following 2000-step minimization, the systems were equilibrated in the NpT (constant number of particles, pressure, and temperature) ensemble using Nosé−Hoover Langevin piston pressure control[52] for 2 ns. In all simulations, the temperature was maintained at 295 K using a Langevin thermostat with a damping constant of 1.0 ps^{-1} applied to the heavy atoms of the lipid membrane.

dx.doi.org/10.1021/jp111441p |*J. Phys. Chem. C* XXXX, XXX, 000–000

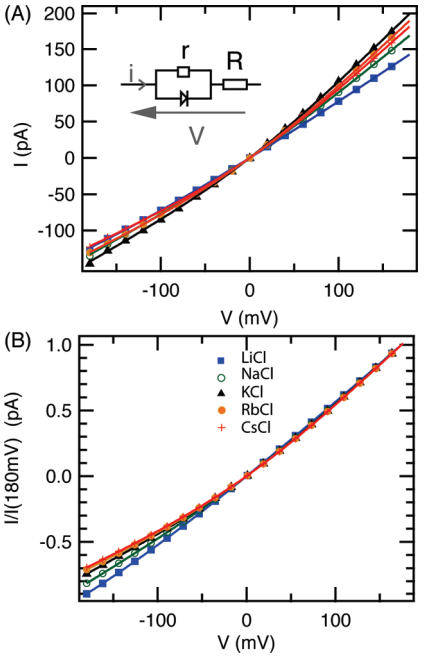

Figure 1. (A) $I-V$ curves of α-hemolysin for the five alkali chloride solutions: Li^+ (solid squares), Na^+ (empty circles), K^+ (solid triangles), Rb^+ (solid circles), Cs^+ (+). Fits of the data to the electrical circuit model, eq 1, which is schematically shown in the inset, are plotted as continuous color lines. At positive voltages, the highest current is obtained for potassium and the lowest for lithium electrolytes. At negative voltages, the currents are almost independent of the ion type. (B) The ionic current normalized by its value at 180 mV. The five curves overlap in the positive voltage region due to their linear shape. In the negative voltage region, the current asymmetry increases from Li^+ to Cs^+.

All production simulations were carried out in the *NVT* (constant number of particles, volume, and temperature) ensemble, with an external electric field applied perpendicular to the lipid layer. In contrast to our previous work,[35] all C_α atoms of the protein were harmonically restrained to their X-ray coordinates using the spring constant of 695 pN/nm, which was necessary to prevent sporadic structure deterioration. All five systems (LiCl, NaCl, KCl, RbCl, and CsCl) were simulated at a ±600 mV transmembrane bias. Additional simulations were performed at ±1.2 V and ±180 mV for the LiCl, NaCl, and KCl systems only. The typical duration of our MD trajectories varied between 20 and 30 ns for 600 mV and 1.2 V bias simulations and was at least 100 ns at 180 mV . The ionic currents were calculated as described previously.[35]

RESULTS

First, we present measurements of $I-V$ curves of α-hemolysin for 1 M alkali chloride solutions between −180 and +180 mV. The voltage dependence of the pore conductance and of the current rectification is characterized for each alkali chloride buffer. Following that, we show that all-atom MD simulations can reproduce the results of the measurements and analyze the MD trajectories to determine the molecular origin of the current rectification.

Experiment. Figure 1 displays the $I-V$ curves of α-hemolysin for all 1 M alkali chloride solutions at pH 7.4. All the curves are asymmetric with respect to the applied voltage, and the conductances are of the order of 1 nS. Notice that this value is a factor 5 to 10 smaller than the conductance of a cylinder 1.8 nm in diameter and 5 nm in length filled with bulk electrolyte. In the following, we provide more detailed analysis of the pore conductivities and current rectification.

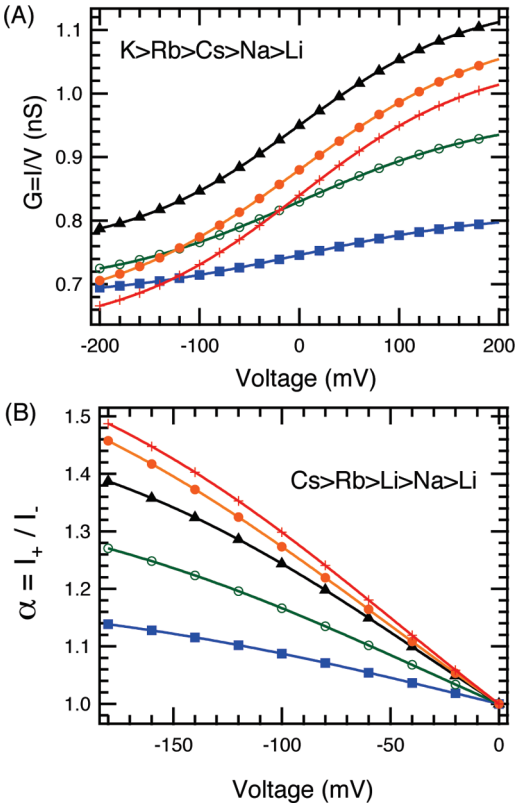

Figure 2. Experimental voltage-dependent conductance of α-hemolysin $G_{pore} = I/V$ (A) and the asymmetry factor $(I_+)/(I_-)$ (B) measured using 1 M solution of Li^+ (solid squares), Na^+ (empty circles), K^+ (solid triangles), Rb^+ (solid circles), and Cs^+ (+) chloride.

Pore Conductance. We define the conductance, G_{pore}, as the ratio of the ionic current, I, to the applied voltage, V: $G_{pore} = I/V$. To properly characterize the voltage dependence of the pore conductance, especially in the $V\sim0$ regime, we fit our data to the electrical model schematically shown in the inset of Figure 1. The model consists of a diode with a leak resistance r in series with another resistance R. The diode characteristic is taken as $I = I_0(\exp(U/V_0) - 1)$. This electrical analogy corresponds to a situation where the access energy barrier for an ion to move through the pore is of the order of k_BT, producing partial rectification of the current. Although this model is not without physical grounds, we use it here primarily to analyze and discuss the results of our measurements. Our experimental $I-V$ curves were fitted by solving the following implicit equation

$$I = \frac{V}{r+R} + \frac{rI_o}{r+R}\left[\exp\left(\frac{V-RI}{V_o}\right) - 1\right] \qquad (1)$$

As shown in Figure 1, this expression perfectly fits our experimental data. The parameters of the fit are listed in Table 1.

The measured conductances are displayed in Figure 2(A) as a function of the applied voltage V for all alkali cations. The conductance of α-hemolysin is voltage dependent and increases continuously from −180 to +180 mV. The conductance saturates in the limit of large positive and negative voltages. Using our model, we can determine the conductance at a large positive

dx.doi.org/10.1021/jp111441p |*J. Phys. Chem. C* XXXX, XXX, 000–000

voltage as $G_{+\infty} = 1/R$ and at a large negative voltage as $G_{-\infty} = (1)/(R+r)$ for each cation type.

Previous experimental studies of α-hemolysin in KCl solutions of various concentrations have shown that the pore conductance scales as the conductivity of the bulk electrolyte.[53] A naive expectation would then be that the pore conductances $G_{pore}(V)$ scale or at least rank in the lyotropic order $Li^+ < Na^+ < K^+ < Rb^+ < Cs^+$. Instead we find that the pore conductances rank as $Li^+ < Na^+ < Cs^+ < Rb^+ < K^+$ for a constant ionic strength. Figure 2(A) illustrates this effect: the pore conductance cannot be scaled with the buffer conductivity σ_b over the entire range of voltages. However, the conductance extrapolated to a large positive voltage G_∞ scales within 10% error with σ_b (see Table 1). At a large negative voltage, the conductance $G_{-\infty}$ is almost independent of the cation type. In this limit, we can hypothesize that the current is mainly carried by the common Cl^- anions, whereas at positive voltages the cations significantly contribute to the total current. This hypothesis is further supported by our MD simulations (see next sections). Our measurements are consistent with previous reports of mild anion selectivity of α-hemolysin at neutral pH[54] and with the existence of an energy barrier controlling ion transport at small transmembrane biases.[20]

Current Rectification. We define the current asymmetry factor α as $(I_+)/(I_-)$, where I_+ and I_- are the absolute values of the current at positive and negative voltages. Figure 2(B) shows that α decreases from $(R + r)/(R)$ at large voltages to 1 in the limit $V \sim 0$. For the Li^+ electrolyte, the asymmetry factor is below 1.1, whereas it can rise to 1.4 for the Cs^+ electrolyte. The current rectification hence follows the lyotropic order. As a crude argument to explain this observation, we can build on our hypothesis regarding the change in the constitution of the ionic current at positive and negative voltages. In the case of LiCl, the current is almost symmetric, and thus the cations are expected to carry a minor fraction of the current. In contrast, the higher rectification degree for the Cs^+ ions would indicate that in this case the cation contributes significantly to the current at a positive bias. Our MD simulations provide support to this interpretation and detail the mechanism of the selective cation transport at the atomic level.

Simulation. The simulated $I-V$ curves of α-hemolysin for 1 M LiCl, NaCl, and KCl electrolytes are displayed in Figure 3(A). The inset shows the experimental $I-V$ curves in the range of −180 to +180 mV. The lines in Figure 3(A) show extrapolation of the experimental $I-V$ curves to [−1.2 V, +1.2 V] interval using eq 1 and parameters from Table 1. The currents at negative voltages appear to be almost independent of the cation type in both experiment and simulations. At positive biases, the simulated currents increase as the electrolyte changes from LiCl to NaCl and to KCl. Figure 3(B) shows the same data scaled by the current value at +1.2 V. The $I-V$ curve of KCl exhibits the greatest asymmetry, while that of LiCl appears symmetric. Despite some minor quantitative discrepancies, the simulated and measured $I-V$ curves appear to be in good agreement.

Figure 4 provides a quantitative assessment of the accuracy of our MD method. The simulated and measured conductivities of 1 M bulk electrolytes are plotted in Figure 4(A). The simulated bulk conductivities differ from experimental values by a factor 1.1 to 1.8, depending on the type of the electrolyte. Note that the use of rigid water model increases the conductivity of KCl at 1 M if compared to that reported in previous studies.[35,55] Figure 4(B) displays the asymmetry factor computed using the above

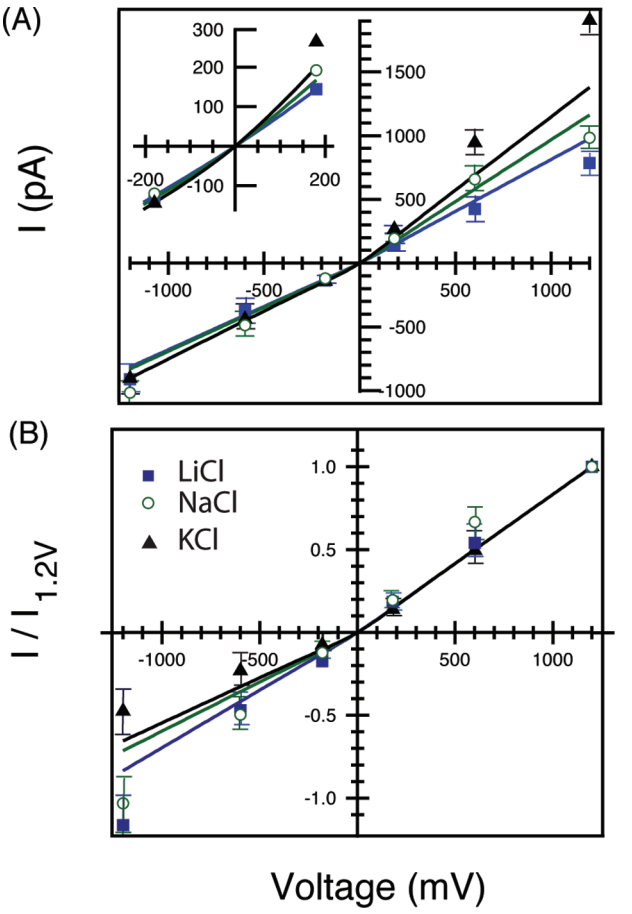

Figure 3. (A) Simulated $I-V$ curves of α-hemolysin for 1 M solutions of LiCl (solid squares), NaCl (empty circles), and KCl (solid triangles). Experimental curves measured in the [−180 mV, +180 mV] range are plotted in the inset. The continuous lines in both the inset and the main panel are obtained by extrapolating the experimental values over the simulation voltage range using eq 1 and the best fit parameters listed in Table 1. (B) Same data scaled by the value of the current at 1.2 V.

conductance values. The simulated asymmetry factor is in a good qualitative agreement with experiment; however, the quantitative agreement of unscaled values is rather poor due to overestimation of KCl, RbCl, and CsCl conductances.

Figure 4 (C),(D) shows the simulated conductances at ±600 mV bias. As experimentally observed, they rank as $G_{LiCl} < G_{NaCl} < G_{KCl} \approx G_{RbCl} \approx G_{CsCl}$ for the positive voltage and hardly depend on cation types for the negative voltage. Scaling the simulated conductance with the ratio of measured and simulated bulk conductivities significantly improves agreement between simulation and experiment at +600 mV and, to a lesser degree, at −600 mV. Thus, the overestimation of the pore conductance in the MD simulations is related to the systematic overestimation of the bulk conductivity, which is the intrinsic property of the MD force field. However, as the relative contribution of cations and anions to the total ionic current depends on the magnitude and polarity of the transmembrane bias,[35] scaling the $I-V$ curve with a single factor cannot be expected to yield good quantitative agreement in the entire voltage range. Despite all these shortcomings, our simulations reproduce the experimental observations at a semiquantitative level, indicating that the physics of

dx.doi.org/10.1021/jp111441p |J. Phys. Chem. C XXXX, XXX, 000–000

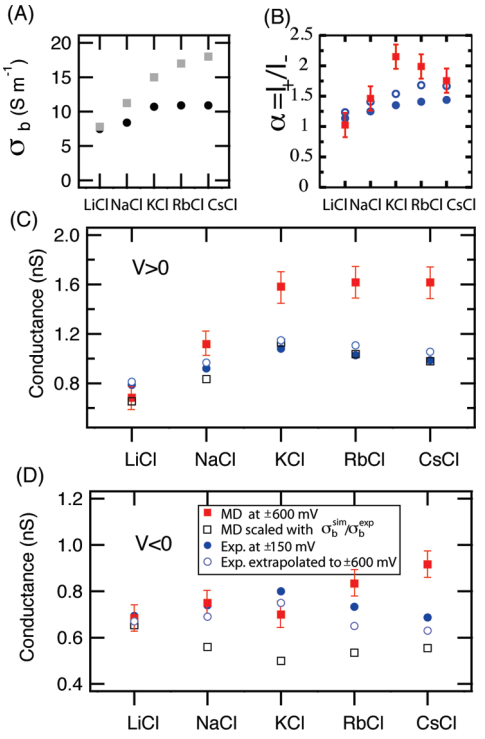

Figure 4. Quantitative comparison of experimental and simulated conductances of the five alkali electrolytes. (A) Simulated (squares) and measured (circles) conductivities of 1 M bulk electrolytes. (B) The asymmetry factor, $(I_+)/(I_-)$, predicted from MD simulations at ±600 mV (solid squares), measured in experiment at ±150 mV (solid circles), and extrapolated to ±600 mV (open circles). (C) The conductance of α-hemolysin obtained from MD simulations at +600 mV (solid squares) and corrected by the ratio of experimental and simulated bulk conductivities (empty squares), measured in experiment at +150 mV (solid circles), and extrapolated to +600 mV (empty circles). (D) The conductance of α-hemolysin at negative biases. The symbols have the same meaning as in (C).

interactions that cause cation type-dependent rectification of the ionic current are correctly captured by our MD approach.

■ ANALYSIS AND DISCUSSION

In the previous section, we have shown that our MD simulations could reproduce the experimental observations with semi-quantitative accuracy. As the position of every atom in the simulation system is known at every simulation time step, it is possible to determine the molecular mechanism of the current rectification phenomena by analyzing the MD trajectories.

Let us first examine how the currents carried by cationic and anionic species are affected by a reversal of the transmembrane bias. Figure 5 shows the fraction of the total current carried by cations for the following three electrolytes: LiCl, NaCl, and KCl. At negative biases, the current of cations is considerably smaller than that of Cl^-. Furthermore, the cation current does not appear to depend on the magnitude of the bias. Li^+ has the smallest fractional current (<10%), whereas the fractional currents of Na^+ and K^+ are about 14 and 27%, respectively. Thus, at negative biases, the current is carried mostly by Cl^-, which is consistent with the experimental $I-V$ curve, Figure 1(A), that shows that the current at negative biases does not depend on the cation type. At positive biases, the fractional current of cations

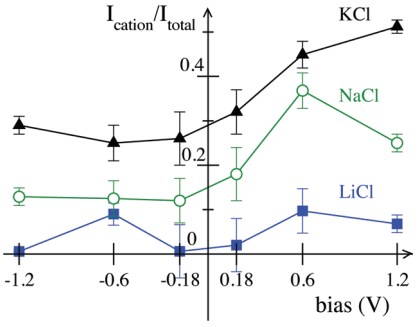

Figure 5. Fraction of the total ionic current through α-hemolysin carried by cations in the case of LiCl (solid squares), NaCl (empty circles), and KCl (solid triangles).

increases with the bias in the case of NaCl and KCl, but not LiCl. Table S1 in the Supporting Information which lists the chloride and the cationic currents of the five systems at ±0.6 V reveals that the chloride current decreases slightly when the bias is reversed. However, this variation is not significant compared to the change in the cationic current. Hence, the asymmetry of the $I-V$ curves appears to be closely related to the change in the current of cations upon reversal of the transmembrane bias. Below we determine which properties of the channel and the electrolytes produce this effect.

Simple Quantitative Model of Ion Conductance. In a steady state, the average ionic current is constant everywhere in the pore. We chose to focus our analysis on a nearly cylindrical region 36 Å in length positioned between the *trans* entrance of the stem and the constriction of the stem-vestibule juncture (see Figure 6(A)). This region is further referred to as the stem region.

Ion Mobility. It is quite reasonable to expect that the mobility of an ion changes as it enters the pore of α-hemolysin from the bulk. To estimate this effect, we performed a set of MD simulations that characterized the mobility of ions in the bulk electrolytes and in the stem region. Table 2 lists the bulk mobility of the ions μ_b^{sim} evaluated from its definition $v_r = \mu_b^{sim} E$, where v_r is the velocity of an ion with respect to the solvent and E is the electric field. The simulated bulk mobilities are within 5−17% of the experimental values μ_b^{exp} and follow the expected lyotropic order.

The same method could, in principle, be used to obtain the position-dependent mobility inside the α-hemolysin pore. However, the inhomogeneous distribution of the electrostatic field and the small number of charge carriers make this approach impractical due to large statistical errors. Therefore, to assess the effect of the pore on the ion mobility, we carried out two sets of simulations, in which the same ions were dragged through the pore of α-hemolysin and through bulk electrolyte under a constant force of 69.47 pN and no external electric field applied.

To obtain good quantitative assessment of the average velocity of the dragged ions in the stem of α-hemolysin, the constant force simulations were performed 16 times for each ion type (eight times in each direction) with the ion initially located outside the boundaries of the stem region. In the limit of low ion concentration, the mobility of an ion can be evaluated from these simulations as $\mu = F/vq$ where F is the applied force; q is the charge of the ion; and v is its average velocity. However, as this approach does not take into account the hydrodynamic effects arising from correlated motion of ions in high-concentration electrolytes, a more accurate estimate is $\mu_{pore}^{eff} = \mu_b^{sim} v_{pore}/v_{bulk}$, where we assumed that the ratio of ion velocities in the pore and

dx.doi.org/10.1021/jp111441p | J. Phys. Chem. C XXXX, XXX, 000–000

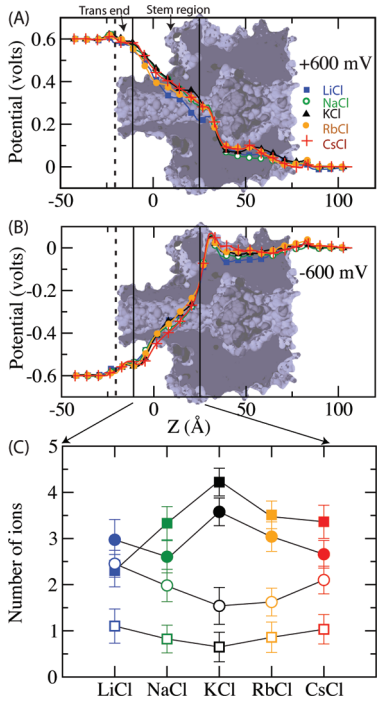

Figure 6. Average electrostatic potential in the pore of α-hemolysin at +600 (A) and −600 (B) mV transmembrane bias in MD simulations of α-hemolysin at 1 M LiCl (solid squares), NaCl (empty circles), KCl (solid triangles), RbCl (solid circles), and CsCl (+). The black vertical lines define the stem region (between −11 and 25 Å) that we considered in our quantitative analysis. The vertical dashed and solid lines define the volume of the *trans* end. (C) The average number of ions in the stem region of α-hemolysin defined by the vertical black lines in panels (a) and (b). The solid and open squares indicate the average number of cations at +600 and −600 mV, respectively. The solid and open circles show the same data for Cl^-. Lines are guides to the eyes. The data for LiCl, NaCl, and KCl simulations at ±180 mV are shown in Figure S1 in the Supporting Information.

Table 2. Measured (μ_b^{exp}) and Simulated (μ_b^{sim}) Ion Mobilities in 1 M Bulk Electrolytes[a]

cations	μ_b^{exp}	μ_b^{sim}	v_{pore}/v_{bulk}	μ_{pore}^{eff}
Li^+	4.01	3.45	0.30	1.03
Na^+	5.19	4.29	0.38	1.63
K^+	7.62	7.66	0.56	4.29
Rb^+	7.92	8.32	0.43	3.59
Cs^+	8	8.98	0.47	4.25
Cl^-		7.32	0.47	3.44

[a] v_{pore}/v_{bulk} is the ratio of ion velocities in the stem of α-hemolysin and in the bulk when the ion is subject to the same mechanical force. $\mu_{pore}^{eff} = \mu_b^{sim} v_{pore}/v_{bulk}$. The mobilities are expressed in 10^{-8} m^{-2} s^{-1} V^{-1}.

in the bulk, v_{pore}/v_{bulk}, is the same when the ion is driven by a constant electric field or a constant mechanical force. Table 2 lists computed effective ion mobilities, μ_{pore}^{eff}, which are 2- to 3-fold less than the ion mobilities in the bulk.

Distribution of the Electrostatic Potential. Figure 6(A),(B) plots the average electrostatic potential inside the central pore of α-hemolysin at ±600 mV computed using the method described elsewhere.[35] For all five electrolytes, the electrostatic profiles at the same voltage bias appear to be almost identical, with a mild

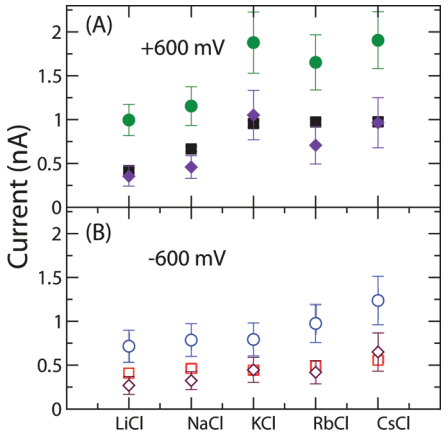

Figure 7. Test of the quantitative model of ion conductance. The simulated ionic currents are shown as filled and open squares at +600 (A) and −600 (B) mV bias, respectively. Also shown are the values of the ionic current computed from eq 2 using the simulated ion mobilities in bulk electrolytes (circles) and the effective ion mobility estimated from constant force pulling simulations (diamonds). The ion mobilities are listed in Table 2. The data for LiCl, NaCl, and KCl simulations at ±180 mV are shown in Figure S3 in the Supporting Information.

energy barrier near the pore constriction and an almost linear drop in the stem region that we chose for our analysis. However, the slope of the linear drop and hence the effective driving force applied to the ions was found to depend on the polarity of the bias: −11.5 ± 0.4 pN/e at +600 mV and 14.9 ± 0.4 pN/e at −600 mV. Similar distributions of the electrostatic potential are observed at ±180 mV (Figure S1, Supporting Information). Note that the asymmetry of the electric field cannot explain the current rectification since the field is larger at negative voltages when the observed currents are smaller. Thus, the current asymmetry should stem from the asymmetry of the concentration of charge carriers.

Ion Concentration. The variation of the ion concentration along the pore axis at ±600 mV is characterized in Figure S2 in the Supporting Information. Figure 6 c plots the average number of anions and cations within the stem region chosen for our analysis. Whereas the number of ions in an equivalent volume of 1 M bulk electrolyte is about 6.5, the number of ions in the stem region is considerably smaller and depends on both the polarity of the bias and the type of the electrolyte. At the positive bias, the number of cations varies between 3 and 4 depending on the ion type, whereas at the negative bias, it is about 1 or smaller. The number of chloride ions also depends on the polarity of the bias and the electrolyte type but to a smaller degree. At the positive bias, the number of cations is in slight excess over the number of chloride ions, and hence the stem region carries a small positive charge. The situation is reversed at the negative bias, as the chloride ions outnumber cations. Similar occupancy of the stem was observed in our simulations of LiCl, NaCl, and KCl at ±180 mV, which are characterized in Figure S1c in the Supporting Information. The above observations are consistent with the data presented in Figure 5 that show that the current at negative biases is primarily carried by Cl ions.

Quantitative Model. Taking into account a linear drop of the electrostatic potential in the volume of interest (the stem region) and a nearly constant ion concentration (Figure S2, Supporting Information) that we further approximate by introducing the

dx.doi.org/10.1021/jp111441p | *J. Phys. Chem. C* XXXX, XXX, 000–000

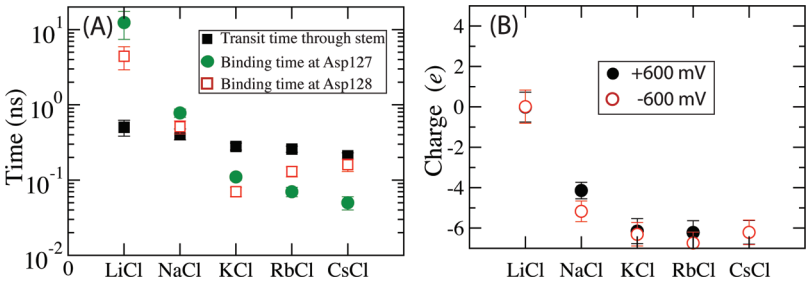

Figure 8. (A) Average transit time of cations through the stem of α-hemolysin (solid black squares) compared with the average binding time of cations to residues Asp127 (solid green circles) and Asp128 (empty red squares) in MD simulations at +600 mV bias. (B) The effective charge of the trans end of the stem at +600 mV (solid circles) and −600 mV (empty circles). The nominal charge of the channel (−7*e*) is partially neutralized by transient binding of ions (see text). The data for LiCl, NaCl, and KCl simulations at ±180 mV are shown in Figure S4 in the Supporting Information.

average number of ions in that volume, N_i, the ionic current I can be computed as

$$I = \frac{e}{L}\sum N_i \mu_i \frac{\Delta V}{L} \qquad (2)$$

where e refers to the electric charge, i to the ion types, and ΔV to the potential drop across the region of interest which is of length L. Figure 7 compares the predictions of the above model to the ionic currents observed in our simulations at ±600 mV bias. Using the bulk mobility of the ionic species μ_b^{sim}, eq 2 overestimates the simulated currents by more than 2-fold. However, replacing the bulk mobility with the effective mobility in the pore μ_{pore}^{eff} (see above) produces results that are in excellent agreement with the simulation data. Good agreement of the above model with the simulation data was also observed in our simulations of LiCl, NaCl, and KCl at ±180 mV, which are characterized in Figure S3 in the Supporting Information.

Having established that the above model quantitatively describes our simulation data, we can now conclude that the variation in the number of ions observed upon a reversal of the transmembrane bias and its dependence on the type of the electrolyte produce the cation-type dependent rectification of the ionic current. We investigate below how this ion number variation comes about from the microscopic structure of the channel.

Molecular Origin of the Cation Type-Specific Current Rectification. Using Brownian dynamics and Poisson−Nernst−Planck modeling, Noskov and Roux have already investigated the microscopic origin of the current rectification in α-hemolysin, demonstrating the critical role of charged residues at the *trans* entrance of the pore (Asp127, Asp128, and Lys131).[34] In particular, they found that the net negative charge (−7*e*) of the *trans* end of the pore is the single dominant factor that determines the asymmetric shape of the *I*−*V* curve in the case of the KCl electrolyte.

Building on these results, we hypothesized that the cation type-dependent asymmetry of the *I*−*V* curves originates from a different ability of cations to screen the negative charge of the pore. To estimate this effect, we evaluated the average number of cations bound to residues Asp127 and Asp128 and the average duration of the cation binding.

For our analysis, we defined an ion as being bound if it resided within a cutoff distance from the same residue in the two consecutive frames of the MD trajectory (sampled every 10 ps). The cutoff values used in our analysis varied between 2.5 Å for Li^+ and 3.5 Å for Cs^+ and were extracted from a pair correlation analysis of the cations and the carboxylate group of residues Asp127 and Asp128. Having identified all the ion-residue pairs, we evaluated the lifetime of each pair and from these data computed the average ion binding time. The same MD trajectories were used to determine a typical time required for an ion to transit the stem of the pore, the average transit time.

Figure 8(A) compares the average binding time with the average transit time for all five cation types. The binding time of Li^+ ions by far exceeds the binding time of all other cations and is considerably longer than the typical ion transit time. For K^+, Rb^+, and Cs^+, the binding time is smaller than the transit time, and for Na^+ ions, the two time scales are comparable. A similar analysis of Cl^- binding to Lys131 revealed that the number of bound Cl^- is nearly zero for all electrolyte types.

To quantitatively assess the influence of ion binding on the effective charge of the α-hemolysin pore, we computed the average number of ions that remained bound to the *trans* end of the pore longer than a typical ion transit time, which at ±600 mV is about 100 ps. Figure 8(B) plots the effective charge of the *trans* end of the stem after taking into account the ion binding. In the case of LiCl, the *trans* entrance of the stem is electrically neutral because of Li^+ binding to Asp127 and Aps128. For NaCl, the effective charge of the trans end varies between −4 and −5 *e*, whereas for KCl, RbCl, and CsCl, the ion binding has very little effect on the pore charge. The simulations performed at ±180 mV reveal a similar dependence (Figure S4, Supporting Information). Thus, binding of Li^+ to the charged residues of the stem should have an effect similar to pore neutralization by mutation, a prediction that we test in the next section.

Further analysis of the MD trajectories brings more insight into the molecular mechanism of the current rectification. Figure 9(A) shows that the current of cations increases in the order LiCl < NaCl < KCl ∼ RbCl ∼ CsCl at a bias of 600 mV. This corresponds to a similar variation of the number of ions in the stem at the same bias (Figure 6(C)). The current of Cl^- varies considerably less in different electrolytes at the same bias. The dependence of the I−V curve on the electrolyte type may therefore be attributed to the variation of the cationic current in the forward (V > 0) direction. Since cations enter the stem segment at a positive bias from the *trans* entrance, the number of cations at the *trans* entrance should depend on the electrolyte type.

Indeed, Figure 9(B) shows that the number of mobile ions at the *trans* end of the channel (defined as the difference between the total number of ions and the number of ions bound to the pore) depends on the type of the electrolyte. Note that the number of cations and anions in the *trans* entrance (Figure 9(B)) is almost invariant upon reversal of the bias which is in sharp contrast to the number of ions (particularly cations) in the stem (Figure 6(C)).

dx.doi.org/10.1021/jp111441p |*J. Phys. Chem. C* XXXX, XXX, 000–000

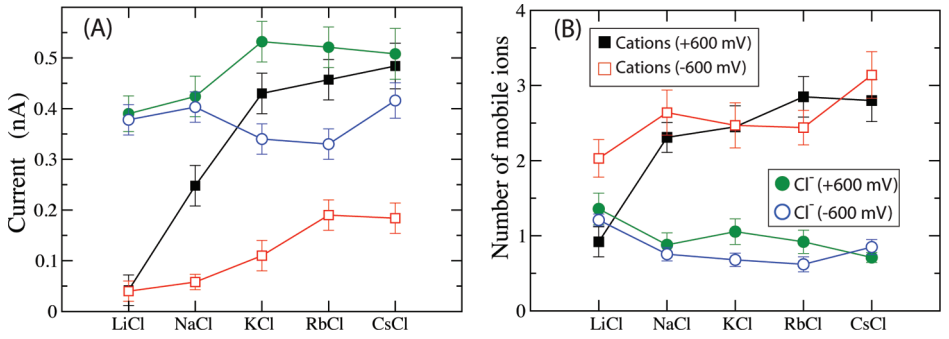

Figure 9. (A) Cationic (squares) and Cl^- (circles) currents recorded in the MD simulations of the wild-type α-hemolysin at +600 (solid symbols) and −600 mV (empty symbols) bias for the five electrolytes. (B) The average number of mobile cations (squares) and Cl^- (circles) at +600 mV (solid symbols) and −600 mV (empty symbols) in the volume of the *trans* end of the pore defined in Figure 6(A). The number of mobile ions is defined as the difference between the total number of ions and the number of ions bound to the pore in the given region. Lines are guides to the eyes.

Table 3. MD Simulations of the Wild-Type and Mutant Variants of α-Hemolysin

		current (nA) (+0.6 V bias)			current (nA) (−0.6 V bias)			asymmetry factor
electrolyte	protein	I_{Cat}	I_{Cl}	I_{Tot}	I_{Cat}	I_{Cl}	I_{Tot}	I_+/I_-
KCl	WT	0.43	0.53	0.96 ± 0.05	−0.11	−0.34	−0.45 ± 0.07	2.1 ± 0.4
	N	0.27	0.48	0.75 ± 0.05	−0.24	−0.60	−0.84 ± 0.05	0.9 ± 0.1
	Asp127P	0.19	0.64	0.83 ± 0.05	−0.21	−0.78	−0.99 ± 0.05	0.8 ± 0.1
	Asp128P	0.31	0.49	0.8 ± 0.06	−0.18	−0.48	−0.66 ± 0.05	1.2 ± 0.2
LiCl	WT	0.04	0.40	0.44 ± 0.05	−0.04	−0.38	−0.42 ± 0.04	1.04 ± 0.2
	N	0.09	0.39	0.48 ± 0.05	−0.005	−0.57	−0.575 ± 0.05	0.8 ± 0.12

Effect of Point Mutations. To test our conclusions, we investigated the influence of the point mutations on the ion conductance of α-hemolysin using our all-atom MD method. Due to the large computational expense of the MD simulations, we limited our study to the case of KCl and LiCl and the following three modifications, (i) protonation of Asp127 (Asp127P), (ii) protonation of Asp128 (Asp128P), and (iii) simultaneous protonation of Asp128 and Asp128 and deprotonation of Lys131, that we refer to as the neutral triple mutant (N). These particular modifications were chosen because they all neutralize the charge of the *trans* end of the stem and minimally distort the geometry of the channel.

Table 3 lists the currents obtained from the MD simulations of the mutant structures at ±600 mV bias. Only the triple mutant was simulated with LiCl. In the case of KCl, the simulations have showed that neutralization of the charges at the *trans* entrance of the pore significantly reduces the cation current at the positive bias and enhances the Cl^- current at the negative bias, with little effect on the Cl^- current at the positive bias and cation current at the negative bias. At the molecular level, the above changes in the pore current can be explained by the attractive (cations) and repulsive (Cl^-) electrostatic forces between the ions and the negatively charged *trans* end of the wild-type (WT) pore. The asymmetry factor α decreases from 2.1 of the WT pore to 1.2 for Asp128P, 0.8 for Asp127P, and 0.9 for the N mutants in the case of KCl. Thus, neutralizing the *trans* end of the channel removes or even slightly reverses the asymmetry of the $I-V$ dependence, which is consistent with the results of BD simulations.[34] The influence of the mutations is much less dramatic in the case of LiCl, with the asymmetry factor changing from 0.95 for WT to 0.83 for the N mutant. The modest rectification that remains after neutralization of the *trans* end of the channel can be attributed to the asymmetric distribution of the charged residues near the constriction of the stem-vestibule juncture.[34]

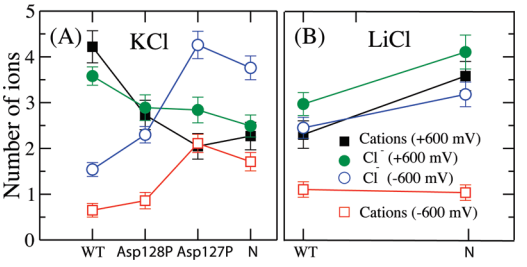

Figure 10. Number of cations (squares) and anions (circles) in the stem of the pore at +600 mV (solid symbols) and −600 mV (empty symbols) observed in the MD simulations of wild-type and mutant variants of α-hemolysin (see text) with (A) KCl and (B) LiCl electrolytes. Lines are guides to the eyes.

The data presented in Table 3 show that neutralization of the *trans* end of the stem does not alter the anion selectivity of the channel: the mutant pores exhibit a larger Cl^- than cation currents, particularly at negative biases. This is consistent with the results of the BD simulations,[34] which have identified the interaction of the ions with the constriction of the channel at the juncture of the stem and the vestibule as the cause of anion selectivity. The low current of cations, particularly at negative biases, can be associated with the sharp increase of the electrostatic potential in the constriction of the channel (Figure 6 and Figure S1, Supporting Information).

We have used the results of these simulations to verify our conclusion that the dominant effect of having the net charge at the *trans* end of the stem is modulation of the number of ions in the stem. Figure 10 displays the average number of ions in the

dx.doi.org/10.1021/jp111441p |*J. Phys. Chem. C* XXXX, XXX, 000–000

stem of the WT and mutant channels. In the case of KCl, the variation in the number of cations in the stem upon a reversal of the transmembrane bias is less dramatic when the *trans* end of the stem is neutralized. Furthermore, a clear correlation between the asymmetry factor, Table 3, and the change in the number of potassium ions in the stem, Figure 10, is apparent. The change in the number of chloride ions shows the same trend, reversing the sign for Asp127P and N mutants. In the case of LiCl, the mutations cause a rather modest change in the average number of ions in the stem. Thus, our simulations of the mutant pores have shown a clear interdependence between the charge of the *trans* end of the stem, the number of ions in the stem, and the ionic current. Removal of the excess negative charge from the *trans* end of the WT pore was observed to increase the number of Cl^- ions entering the stem from the *trans* side at a negative bias and reduce the number of cations entering the stem from the *trans* side at a positive bias.

CONCLUSIONS

In this study, we experimentally characterized the rectification properties of α-hemolysin channels for all alkali buffers at 1 M. Using all-atom MD simulations, we could semiquantitatively reproduce the channel conductances and rectification degree for all alkali salts. We characterized the effective mobility of the alkali ions in the pore, the local electrostatic potential, and the local ion concentration. We demonstrated that cation-dependent rectification of the ionic current originates from a change in the cation concentration in the stem region of α-hemolysin. The latter arises from the different ability of cations to screen the charged residues of the pore (high screening for Li^+ and low screening for Cs^+). To our knowledge, this work is the first quantitative test of the new molecular force field[49] for the entire alkali series in the context of ion transport through narrow channels. Despite some quantitative discrepancies, we found the results of our MD simulations to be in good agreement with the results of the measurements, enabling subsequent studies of the effects of alkali salts on nanopore transport of biomolecules.

In the context of nanopore experiments, this study is the first step toward enhancing the discriminative power of nanopore sensors by fine-tuning physical properties of the electrolyte. For instance, the α-hemolysin nanopore has been the subject of vigorous research in DNA sequencing applications. Most experiments have used KCl as the electrolyte for historical reasons. On the basis of our observations that the cationic current is strongly influenced by the interaction of the ions with the pore, we may conjecture that there would also be a variation in the manner in which the cations interact with different molecules placed in the pore which could be exploited for different applications. Future studies will determine how different electrolytes can be used to improve the detection capability of nanopore sensors.

ASSOCIATED CONTENT

Supporting Information. Additional experimental details. This material is available free of charge via the Internet at http://pubs.acs.org.

AUTHOR INFORMATION

Corresponding Author

*E-mail: aksiment@illinois.edu; virgile.viasnoff@espci.fr.

ACKNOWLEDGMENT

J.M, L.P, J.M., and V.V. are supported by the ANR Grant PNano 06-NANO-015. S.B. and A.A. are supported by the National Institutes of Health through grant R01-HG005115 and by the National Science Foundations through grant DMR-0955959. The supercomputer time was provided by Teragrid through grant MCA05S028.

REFERENCES

(1) Gouaux, E.; MacKinnon, R. *Science* **2005**, *310*, 1461–1465.
(2) Siwy, Z.; Fulinski, A. *Am. J. Phys.* **2004**, *72*, 567–574.
(3) Cheng, L. J.; Guo, L. J. *Nano Lett.* **2007**, *7*, 3165–3171.
(4) Gracheva, M. E.; Vidal, J.; Leburton, J.-P. *Nano Lett.* **2007**, *7*, 1717–1722.
(5) Cheng, L. J.; Guo, L. J. *Chem. Soc. Rev.* **2010**, *39*, 923–938.
(6) Bezrukov, S.; Vodyanoy, I. *Nature* **1995**, *378*, 362–364.
(7) Bezrukov, S. M. *J. Membr. Biol.* **2000**, *174*, 1–13.
(8) Kasianowicz, J. J.; Brandin, E.; Branton, D.; Deamer, D. W. *Proc. Natl. Acad. Sci. U.S.A.* **1996**, *93*, 13770–13773.
(9) Li, J.; Stein, D.; McMullan, C.; Branton, D.; Aziz, M. J.; Golovchenko, J. A. *Nature* **2001**, *412*, 166–169.
(10) Heng, J. B.; Ho, C.; Kim, T.; Timp, R.; Aksimentiev, A.; Grinkova, Y. V.; Sligar, S.; Schulten, K.; Timp, G. *Biophys. J.* **2004**, *87*, 2905–2911.
(11) Storm, A. J.; Chen, J. H.; Ling, X. S.; Zandbergen, H. W.; Dekker, C. *J. Appl. Phys.* **2005**, *98*, 014307–1.
(12) Wanunu, M.; Sutin, J.; McNally, B.; Chow, A.; Meller, A. *Biophys. J.* **2008**, *95*, 4716–25.
(13) Lee, C. Y.; Choi, W.; Han, J.-H.; Strano, M. S. *Science* **2010**, *329*, 1320–1324.
(14) Aksimentiev, A. *Nanoscale* **2010**, *2*, 468–483.
(15) Akeson, M.; Branton, D.; Kasianowicz, J. J.; Brandin, E.; Deamer, D. W. *Biophys. J.* **1999**, *77*, 3227–3233.
(16) Meller, A.; Nivon, L.; Brandin, E.; Golovchenko, J.; Branton, D. *Proc. Natl. Acad. Sci. U.S.A.* **2000**, *97*, 1079–1084.
(17) Ho, C.; Qiao, R.; Chatterjee, A.; Timp, R. J.; Aluru, N. R.; Timp, G. *Proc. Natl. Acad. Sci. U.S.A.* **2005**, *102*, 10445–14450.
(18) Banerjee, A.; Mikhailova, E.; Cheley, S.; Gu, L. Q.; Montoya, M.; Nagaoka, Y.; Gouaux, E.; Bayley, H. *Proc. Natl. Acad. Sci. U.S.A.* **2010**, *107*, 8165–8170.
(19) Derrington, I. M.; Butler, T. Z.; Collins, M. D.; Manrao, E.; Pavlenok, M.; Niederweis, M.; Gundlach, J. H. *Proc. Natl. Acad. Sci. U.S.A.* **2010**, *107*, 16060–16064.
(20) Misakian, M.; Kasianowicz, J. J. *J. Membr. Biol.* **2003**, *195*, 137–146.
(21) Cescatti, L.; Pederzolli, C.; Menestrina, G. *J. Membr. Biol.* **1991**, *119*, 53–64.
(22) Siwy, Z. S.; Trofin, L.; Baker, L.; Kohli, P.; Howorka, S.; Trautmann, C.; Martin, C. R. *Biophys. J.* **2005**, *88*, 658a.
(23) Stoddart, D.; Heron, A. J.; Klingelhoefer, J.; Mikhailova, E.; Maglia, G.; Bayley, H. *Nano Lett.* **2010**, *10*, 3633–7.
(24) Cruz-Chu, E. R.; Aksimentiev, A.; Schulten, K. *J. Phys. Chem. C* **2009**, *113*, 1850–1862.
(25) Pastoriza-Gallego, M.; Oukhaled, G.; Mathe, J.; Thiebot, B.; Betton, J.; Auvray, L.; Pelta, J. *FEBS Lett.* **2007**, *581*, 3371–3376.
(26) Schroder, H. *Eur. Biophys. J. Biophys. Lett.* **1985**, *11*, 157–165.
(27) Gillespie, D.; Eisenberg, R. S. *Eur. Biophys. J. Biophys. Lett.* **2002**, *31*, 454–466.
(28) Gillespie, D.; Nonner, W.; Henderson, D.; Eisenberg, R. S. *Phys. Chem. Chem. Phys.* **2002**, *4*, 4763–4769.
(29) Piasecki, J.; Allen, R. J.; Hansen, J. P. *Phys. Rev. E* **2004**, *70*, 021105.
(30) O'Keeffe, J.; Cozmuta, I.; Bose, D.; Stolc, V. *Chem. Phys.* **2007**, *342*, 25–32.
(31) Ramirez, P.; Gomez, V.; Cervera, J.; Schiedt, B.; Mafe, S. *J. Chem. Phys.* **2007**, *126*, 194703.

(32) Constantin, D.; Siwy, Z. S. *Phys. Rev. E* **2007**, *76*, 041202–10.
(33) Millar, C.; Madathil, R.; Beckstein, O.; Sansom, M.; Roy, S.; Asenov, A. *J. Comput. Electron.* **2008**, *7*, 28–33.
(34) Noskov, S. Y.; Im, W.; Roux, B. *Biophys. J.* **2004**, *87*, 2299–2309.
(35) Aksimentiev, A.; Schulten, K. *Biophys. J.* **2005**, *88*, 3745–3761.
(36) Cruz-Chu, E. R.; Aksimentiev, A.; Schulten, K. *J. Phys. Chem. C* **2009**, *113*, 1850–1862.
(37) Pezeshki, S.; Chimerel, C.; Bessonov, A. N.; Winterhalter, M.; Kleinekathofer, U. *Biophys. J.* **2009**, *97*, 1898–1906.
(38) E. Garcia-Gimenez, A. A.; Aguilella, V. *Phys. Rev. E* **2010**, *81*, 021912.
(39) Corry, B.; Kuyucak, S.; Chung, S.-H. *Biophys. J.* **2000**, *78*, 2364–2381.
(40) Merzlyak, P. G.; Capistrano, M. F. P.; Valeva, A.; Kasianowicz, J. J.; Krasilnikov, O. V. *Biophys. J.* **2005**, *89*, 3059–3070.
(41) Viasnoff, V.; Chiaruttini, N.; Bockelmann, U. *Eur. Biophy. J. Biophys. Lett.* **2009**, *38*, 263–269.
(42) Phillips, J. C.; Braun, R.; Wang, W.; Gumbart, J.; Tajkhorshid, E.; Villa, E.; Chipot, C.; Skeel, R. D.; Kale, L.; Schulten, K. *J. Comput. Chem.* **2005**, *26*, 1781–1802.
(43) Darden, T.; York, D.; Pedersen, L. *J. Chem. Phys.* **1993**, *98*, 10089–10092.
(44) Batcho, P. F.; Case, D. A.; Schlick, T. *J. Chem. Phys.* **2001**, *115*, 4003–4018.
(45) Freddolino, P. L.; Schulten, K. *Biophys. J.* **2009**, *97*, 2338–2347.
(46) Miyamoto, S.; Kollman, P. A. *J. Comput. Chem.* **1992**, *13*, 952–962.
(47) Andersen, H. C. *J. Comput. Phys.* **1983**, *52*, 24–34.
(48) MacKerell, A. D.; et al. *J. Phys. Chem. B* **1998**, *102*, 3586–3616.
(49) Joung, I. S.; Cheatham, T. E. *J. Phys. Chem. B* **2008**, *112*, 9020–9041.
(50) Song, L.; Hobaugh, M. R.; Shustak, C.; Cheley, S.; Bayley, H.; Gouaux, J. E. *Science* **1996**, *274*, 1859–1865.
(51) Jorgensen, W. L.; Chandrasekhar, J.; Madura, J. D.; Impey, R. W.; Klein, M. L. *J. Chem. Phys.* **1983**, *79*, 926–935.
(52) Martyna, G. J.; Tobias, D. J.; Klein, M. L. *J. Chem. Phys.* **1994**, *101*, 4177–4189.
(53) Bonthuis, D. J.; Zhang, J. S.; Hornblower, B.; Mathe, J.; Shklovskii, B. I.; Meller, A. *Phys. Rev. Lett.* **2006**, *97*, 128104–4.
(54) Chakraborty, T.; Schmid, A.; Notermans, S.; Benz, R. *Infect. Immun.* **1990**, *58*, 2127–2132.
(55) Chimerel, C.; Movileanu, L.; Pezeshki, S.; Winterhalter, M.; Kleinekathofer, U. *Eur. Biophys. J.* **2008**, *38*, 121–125.